Reports

Molecular Resolution Electron Micrographs of Monolamellar Paraffin Crystals

Abstract. *A liquid helium–cooled cryoelectron microscope, operated to expose the specimen to only a very low electron dose, was used to obtain structural images of monolamellar* n*-tetratetracontane* (n-$C_{44}H_{90}$) *crystals at 0.25-nanometer resolution. These results are in contrast to earlier predictions that such extremely beam-sensitive materials could not be studied directly at this level of detail. Analysis of the resultant lattice images gives direct evidence for crystal bending as well as direct visualization of edge dislocations in this material.*

F. Zemlin, E. Reuber
E. Beckmann, E. Zeitler
Fritz Haber Institut der Max-Planck-Gesellschaft, Faradaweg 4-6, D-1000, Berlin 33, Federal Republic of Germany
D. L. Dorset
Electron Diffraction Department, Medical Foundation of Buffalo, Inc., Buffalo, New York 14203

Recent high-resolution electron microscope images of numerous microcrystalline organic specimens (*1–4*) have yielded important information about the structure of "real" crystals, including direct views of microtwinning (*4*), grain boundaries (*2*), and crystal defects (*5*). The major impediment to this research (*6*) has been the threat of specimen damage induced by the incident beam; hence the samples examined so far have been materials (such as aromatics) that are relatively stable in the electron beam. Direct examination of more beam-sensitive specimens, on the other hand, is commonly thought to be of limited use. For example, at the dose needed to destroy a paraffin crystal at room temperature, it has been predicted (*7*) that only 4-nm resolution would be attainable, a resolution nearly realized in experimental lattice-fringe images of an epitaxially crystallized sample (*8*). We now describe the direct imaging at 0.25-nm resolution of a paraffin crystal cooled by liquid helium and show that information about crystal structure can be obtained at much higher resolution from materials at least 20 times more beam sensitive than phthalocyanine (*9*) (which is stabilized against beam damage by a delocalized π-electron system).

Monolamellar orthorhombic crystals several micrometers in length of the *n*-paraffin *n*-tetratetracontane (n-$C_{44}H_{90}$) were grown by evaporation of a dilute *n*-hexane solution on electron microscope grids covered with a carbon film. Analysis of hk0 electron diffraction intensity data for these crystals revealed (*10*) that the structure is identical to its n-$C_{36}H_{74}$ homolog, for which the x-ray crystal structure is known (*11*). The orthorhombic unit cell edges in this projection are $a = 0.750$ nm and $b = 0.495$ nm.

For the imaging experiments, a Siemens prototype of a helium-cooled cryomicroscope with a superconducting shielding objective lens (*12*) was used, giving a specimen temperature lower than 15 K. As calculated from data for the Agfa 23D56 film used to record the images (*13*), the magnification (×60,000) needed to achieve 0.25-nm resolution required a radiation exposure of 1000e nm^{-2}, or twice the "critical" exposure measured for this specimen (as judged by fading of electron diffraction patterns). The optical density of the film is usefully large (0.28D) at this exposure, and, although some specimen damage is discernible, this greater dose can nevertheless be used for the following reason. As with earlier findings for polyethylene crystals (*14*) cooled to 111 K, the ratio of lattice spacings for our specimen and the relative intensities of the three intense reflections used to form the image did not change at this radiation dose (Fig. 1). Additional exposure of the specimen was avoided by the usual low-dose techniques; that is, suitable crystals were found from electron diffraction patterns (dose rate, 10^{-1}e $nm^{-2}sec^{-1}$), and, when a suitable specimen was found, the shutter above the specimen was closed and the beam deflected alongside the crystal to permit adjustments for focus and

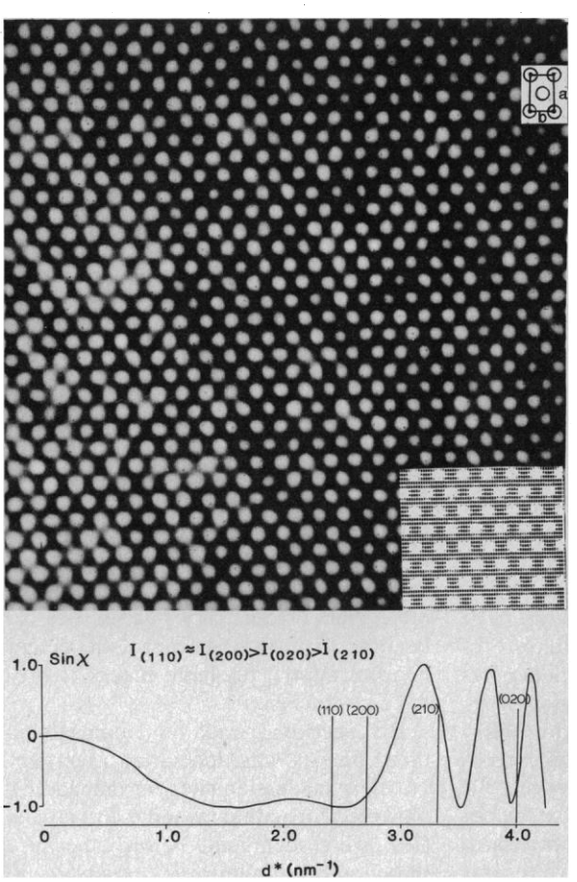

Fig. 1. Lattice images of an *n*-tetratetracontane monolamellar crystal. (Top) Experimental image obtained after cross-correlation averaging. The contrast in this picture is that of the "negative" obtained in the electron microscope that was used for digitization and image processing. White blobs denote the alkane-chain positions (the unit cell is indicated by a white rectangular box). (Inset) Lattice image calculated after an *n*-beam dynamic calculation; $\Delta f = -80.0$ nm, where the negative sign denotes underfocus. These calculations were made with the computer program package available from the Arizona State University facility for high-resolution electron microscopy. The lamellar thickness is 5.77 nm, and the projected slice thickness is 0.25 nm. (Bottom) Phase-contrast transfer function (*25*) for the imaging conditions stated in the text. For resolutions poorer than 0.2 nm, the chromatic aberration and illumination angle do little to modulate the image (*4*) and thus were not included in the represented transfer-function calculation. For the image calculation, however, the illumination angle is defined as 10^{-4} radians. The positions of major reflections are indicated. The phase shift χ is a function of spatial frequency d^*, in accordance with the transfer function equation for the objective lens (*25*).

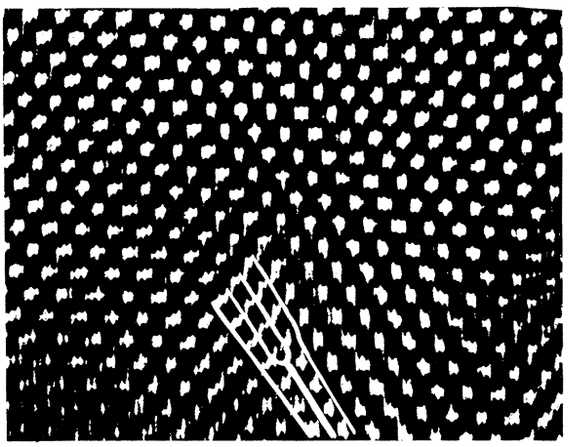

Fig. 2. Section of a "quasi-optically filtered" image, showing an edge dislocation. By analogy to the use of filters in optical image reconstruction, which pass only the maxima of the optical transform, only small circular regions encompassing the maxima of the computed Fourier transform were used to produce this image, thus removing diffuse regions of the transform that were due to noncrystallinity. Chain-position broadening was reproduced by model image calculations. The white lines are added to show the convergence of lattice rows at the dislocation.

astigmatism. After alignment, the beam was deflected onto the specimen to record the low-dose image. At 100 kV, the spherical aberration constant for the objective lens (C_s, 1.35 mm) gave a Scherzer defocus value of −70.7 nm.

Although the electron images were noisy, optical transforms gave diffraction patterns similar in appearance to the electron diffraction patterns, sometimes including the (020) reflection. The area of the micrograph (corresponding to 100 by 100 nm) giving the optical transform with the best symmetry was digitized (by densitometry) as a 1024 by 1024 pixel array. This area was then subdivided into 64 sections, which produced optical transforms of different qualities due to the presence of crystal imperfections or radiation-damaged areas (or both). The subsection with the best optical diffraction symmetry was then cross-correlated with the whole array to localize crystal areas with the greatest structural perfection. These were then aligned and superimposed to produce the image in Fig. 1, which is the average of 372 subregions.

Correspondence of this image to the actual crystal structure was verified by a multislice (*15*) *n*-beam dynamic calculation from the known crystal structure and by subsequent computation of the lattice image at various defocus values. A good match was obtained at $\Delta f = -80.0$ nm (Fig. 1). Computations of the objective lens transfer function revealed that the continuous region of reciprocal space passing diffraction information at the same contrast sign extended to about $(0.33\ \text{nm})^{-1}$. However, the appearance of (020) reflections in the optical transforms resulted from the transfer function being again negative for this $(0.25\text{-nm})^{-1}$ reciprocal spacing (Fig. 1). Thus, because this feature has been used to produce high-resolution images of gold (*16*), it can also be employed here. As shown through image calculations, only the carbon chains were of importance for image production at this resolution; the contribution from hydrogen was small.

The demonstration of molecular resolution is encouraging, especially since the observed image detail can be explained in terms of the known crystal structure and instrumental parameters. However, even more useful information about the crystal texture was given from images (such as the 1024 by 1024 array) produced by a computer simulation of optical filtration than from images averaged by cross-correlation. Observed undulations in the image with changes in contrast were reproduced by image calculations for tilted specimens and thus indicate the presence of bends (this was corroborated by the changes in optical transform symmetry in scans across the image, as mentioned above). Defects such as the edge dislocation (Fig. 2) were also reproduced by an image calculation starting with a defect model proposed by Holland [earlier visualization of such defects with moiré images required at least a bilamellar crystal (*17*)]. These direct visualizations of crystal texture helped confirm earlier conclusions (*10, 18*) that the major distortion in solution-grown molecular organic crystals is due to bending distortion, because the defect concentration is not large enough to produce mosaicism.

Evidence for radiation damage in these images was difficult to ascertain. No clear nucleation sites for damage, as observed for phthalocyanine derivatives (*19*), were identified, perhaps because the damaged structure is initially much like the undamaged one. That is, if the major mechanism is the abstraction of hydrogen and production of *trans*-vinylene groups (*20*), then initial damage would be most visible in a projection onto (but not along) the chain axes, as shown earlier (*21*). Optical transforms of images do not indicate a transition to a pseudohexagonal chain packing [which also is not found as a thermally produced phase for this paraffin (*22*)]. Therefore, Siegel's (*23*) suggestion that initial damage is "frozen in" at low temperature seems to be correct. On the other hand, the recent claim (*24*) of unusual radiation stability for very small (<200 nm in length) paraffin and polyethylene crystals is not understood.

The success of this initial imaging experiment on a highly radiation-sensitive organic is encouraging because of the new insights that can be gained from thin microcrystals of aliphatic polymers for which many aspects of crystallization behavior and crystal texture still need to be elucidated.

References and Notes

1. N. Uyeda *et al.*, *Chem. Scr.* **44**, 4761 (1979); Y. Murata, J. R. Fryer, T. Baird, *J. Microsc.* **108**, 261 (1976).
2. T. Kobayashi *et al.*, *Acta Crystallogr. Sect. A* **37**, 692 (1981); J. R. Fryer, *ibid.* **35**, 327 (1979).
3. J. R. Fryer, *ibid.* **34**, 603 (1978); _____ and D. J. Smith, *Proc. R. Soc. London Ser. A* **381**, 225 (1982); N. Uyeda *et al.*, *Nature (London)* **285**, 95 (1980); M. Tsuji *et al.*, *Polymer* **23**, 1568 (1982).
4. A. Kawaguchi *et al.*, *Colloid Polym. Sci.* **262**, 429 (1984).
5. S. Isoda *et al.*, *Makromol. Chem. Rapid Commun.* **4**, 141 (1983).
6. E. Zeitler, Ed., *Ultramicroscopy* **10**, 1 (1982).
7. R. M. Glaeser, in *Physical Aspects of Electron Microscopy and Microbeam Analysis*, B. M. Siegel and D. R. Beaman, Eds. (Wiley, New York, 1975), pp. 205–229.
8. J. R. Fryer, *Inst. Phys. Conf. Ser.* **61**, 19 (1981).
9. L. Reimer, *Z. Naturforsch. Teil A* **15**, 405 (1960).
10. D. L. Dorset, *Acta Crystallogr. Sect. A* **36**, 592 (1980).
11. P. W. Teare, *ibid.* **12**, 294 (1959).
12. G. Lefranc, E. Knapek, I. Dietrich, *Ultramicroscopy* **10**, 111 (1982).
13. K. H. Downing and D. A. Grano, *ibid.* **7**, 381 (1982).
14. H. Kiho and P. Ingram, *Makromol. Chem.* **118**, 43 (1968).
15. J. M. Cowley and A. F. Moodie, *Acta Crystallogr.* **10**, 609 (1957).
16. H. Hashimoto *et al.*, *Chem. Scr.* **14**, 23 (1979).
17. V. F. Holland, *J. Appl. Phys.* **35**, 3235 (1964); _____ and P. H. Lindenmeyer, *ibid.* **36**, 3049 (1965); V. F. Holland *et al.*, *Phys. Status Solidi* **10**, 543 (1965); M. Niinomi and M. Takayanagi, *Prog. Mater. Sci. Jpn.* **2**, 199 (1971).
18. D. L. Dorset, *Z. Naturforsch. Teil A* **33**, 964 (1978); B. Moss and D. L. Dorset, *Acta Crystallogr. Sect. A* **39**, 609 (1983).
19. J. R. Fryer and F. Holland, *Proc. R. Soc. London Ser. A* **393**, 353 (1984).
20. G. N. Patel, *J. Polym. Sci. Polym. Phys. Ed.* **13**, 351 (1975).
21. D. L. Dorset, F. Holland, J. R. Fryer, *Ultramicroscopy* **13**, 305 (1984).
22. P. K. Sullivan, *J. Res. Natl. Bur. Stand.* **78A**, 129 (1974).
23. G. Siegel, *Z. Naturforsch. Teil A* **27**, 325 (1972).
24. S. Giorgio and R. Kern, *J. Polym. Sci. Polym. Phys. Ed.* **22**, 1931 (1984).
25. K. J. Hanszen, *Adv. Opt. Electron Microsc.* **4**, 1 (1971).

26. Supported by grants from the National Science Foundation (DMR81-16318) and the National Institute of General Medical Sciences (GM21047). We thank the management of Siemens AG, Munich, for putting at our disposal the prototype of a superconducting cryomicroscope.

8 March 1985; accepted 12 June 1985